

## Optical and tribo-mechanical characterization in metal-ceramic multilayers coatings

A. González-Hernández<sup>a</sup>, M. Flores<sup>b</sup>, A. B. Morales<sup>a,\*</sup>, J. C. Caicedo<sup>c</sup>, N.A. de Sánchez<sup>d</sup>, and R. Barragán Ramírez<sup>e</sup>

<sup>a</sup>*Petrochemical Research Center, TecNM/Instituto Tecnológico de Ciudad Madero,  
Parque Tecnia (Pequeña y Mediana Industria) Bahía Aldair Altamira, México.*

*\*e-mail: angonzalez25@hotmail.com*

<sup>b</sup>*Project Engineering Department, CUCEI, Universidad de Guadalajara, Jalisco, México.*

<sup>c</sup>*Tribology, Polymers, Powder Metallurgy and Processing of Recycled Solids Research Group,  
Universidad del Valle, Cali, Colombia.*

<sup>d</sup>*Research Group Materials Science and Engineering, Faculty Engineering,  
Universidad Autónoma de Occidente, Cali, Colombia.*

<sup>e</sup>*Laboratory Materials, Faculty Engineering, Universidad Autónoma de Tamaulipas,  
Campus Tampico-Madero, Tampico Tamaulipas México.*

Received 18 July 2019; accepted 5 May 2020

Laboratory scale studies of tribological properties of nitride coatings are useful in predicting their protective wear behavior in cutting tools for industrial-scale applications. The main aim of this research is to determine optical and tribo-mechanical properties in multilayer coatings of metal-ceramic assigned as coatings A and B. These coatings were deposited by DC magnetron sputtering on carbon steel AISI 1060 using buffer/adhesion layers of W, Ti/W/WN and TiN/TiN respectively. For to determine molecules, interactions of materials were analyzed through of Raman and FTR spectroscopies. The nanohardness, tribological and adhesion behavior were studied by nanoindentation, pin on disk and a tribometer. The hardness and behavior tribological, were obtained by Nano-indentation, pin on disk, and scratch test using a tribometer. FTIR and Raman analysis shown the formation of Ti metallic ion and  $WO_3$  mainly in both coatings. The hardness of coatings shown a slight improvement compared with the substrate. However, for industrial applications this property should be increase. The behavior of COF does not present improvement. The mass loss and wear rate were high significantly due to the formation of cracks on surface coatings. Scratch analysis, it found three wear mechanics determined by the presence of irregular borders with sharp shadow, semicircle detachment in coatings and coatings detachment in the central track as the load increased.

**Keywords:** Multilayer; optical tribo-mechanical properties; magnetron sputtering.

PACS: 81.15.Cd; 81.40.Jj; 81.40.Pq

DOI: <https://doi.org/10.31349/RevMexFis.66.496>

### 1. Introduction

Manufacturing industries work with large machinery (electronics, tools, plastics, etc.). Two scales segment machinery: a) greater scale (as power plants, refineries, petrochemicals) or micro-scale (transistor manufacturer). These machines are prone to use any of their moving parts where they come into contact with various materials. A study carried out in the United Kingdom in 1997, showed that the cost by wear was 650 million Pound Sterling each year, which represented the 0.25% of its annual turnover, [1]. Corrosion and wear are major failure mechanisms that affect performance, safety, and material integrity. The polyvinyl chloride (PVC) polymer manufacturing industry currently presents serious corrosion-abrasion problems due to high-temperature process conditions. The combined effect of wear and corrosion constitutes 5% of the causes of process operating infrastructure failure in this sector, making it the fifth most important degradation mechanism in terms of cost due to premature failure [2,3]. The increase in tool life due to coatings depends on the improved wear resistance at high cutting temperatures due to the reduced friction against the working material and the tool. The area of application of the coatings has been extended to

the last few years, *e.g.*, application on ordinary TiN-coated tool steels. Progress in thin-film preparation techniques has greatly increased the potential application areas for carbides and nitrides since they have a very low coefficient of friction and are very hard [4]. For example, tungsten nitride ( $WN_x$ ) belongs to refractory metal nitrides that have the unique properties of excellent hardness (38.9 GPa), inert chemistry, high melting point, high chemical stability, and thermal conductivity [5]. On the other hand, the titanium-tungsten nitride shows a good tribological behaviour with a low friction coefficient (0.4) [6]. The multilayer is formed by the stacking of layers alternating two materials of different properties. It has been observed that the increase of parallel interlayers on the surface limits the propagation of cracks, allowing the toughness of the set, increasing the number limits phases associated with the decrease of grain size, increasing the toughness. This behavior is ruled by the Hall-Petch equation, which states that the elastic limit of a polycrystalline material ( $\sigma$ ), is determined by the mean grain size ( $d$ ) and ( $\sigma_0$ ) and  $k$  are two experimental constants. The hardness increase in the superior multilayers, is attributed by the law of mixtures, the hardness is given by the average of the two materials, according to the proportion of their respective volumes [7]. For these reasons,

the individual properties of each material are enhanced as a whole in a system providing better properties. On the other hand, AISI 1060 tool grade steel contains carbon 0.55-0.65 %, magnesium 0.60-0.90 %, phosphor < 0.04% and silicon 0.05 %. Rockwell B hardness 1.8 GPa and elastic module 90-210 GPa. It is used in agricultural implements, clutch discs, shafts, arrows, and cutting tools such as knives. Due to the absence of Nickel and Chrome alloys in steel, in contact with the polymeric matrix of Vinyl Chloride, the metal surface shows abrasive wear. One friction experiment carried out by [8], showed that below 60°C, the slip between PVC and steel, the surface damage was negligible. However, as the temperature between the contact pair increases, wear is generated in PVC waste and steel particles 0.444 mg of mass.

This study is the second part of a previously reported results [9], that found for the case XRD, the formation hexagonal structure  $\delta$ -WN and WN phases. The crystal size of both coatings is similar between them (24 nm and 23 nm). Elemental composition was obtained by SEM-EDS containing atomic 50 %; thus, the formation  $W_2N$  is not favorable. The microstructure showed columnar typical growth in the deposition PVD; it observes spherical cones and cracks on the top surface by SEM. The thickness for coating A and B measurements by cross-section SEM, was 6.6 and 6.4 micres, respectively. The grains size obtained by AFM is  $45.3 \pm 1.9$  nm coating A and  $40.4 \pm 0.1$  nm coating B. For the case of dynamic polarization curves the coating A, the current result shows a density ( $1.89 \times 10^{-7}$  A), it tends to be an ennoblement material compared with bare substrate steel. However, in the results obtained from spectroscopy impedance electrochemical showed that the coating B presents a high resistance to polarization ( $30 \text{ K}\Omega \cdot \text{cm}^2$ ). Thus, this experiment consist to study the behavior of Ti and W metallic as buffer layer for adhesion improvement. The compounds of WN and WTiN to improve hardness, corrosion and tribological properties. The experimental design consists of the formation of two blocks of multilayer: The first block multilayers is deposited Ti/W/WN/ WTiN/Ti/ TiN ending with a system multilayer WTiN/W/WN, assigned as coating A. The second block experimental consist to interchanged the position of W, Ti as buffer layer using the next multilayer system W/Ti/TiN/ WTiN/W/WN conserving the similar end multilayer, assigning as coating B. For more details of experimental design, see the A. González's work *et al.*, 2018.

## 2. Materials and method

### 2.1. Materials and substrate preparation

Coatings are obtained through the use of discs 2-in diameter and 0.25-in thickness of Ti and W targets high purity. The substrate used corresponds to AISI 1060 carbon steel, whose elemental chemistry composition is 0.65 % carbon in square plates of  $28 \times 28$  mm and 3 mm of thickness; while, the substrate is for mechanical measurement properties. To determine, the molecular interactions layers were deposited on a

silicon wafer (100). The AISI 1060 substrates were prepared using sandpaper (grain / in<sup>2</sup>) from 100, 220, 600, 1000, 1500, and 2000. For the polish substrate, aluminum oxide ( $Al_2O_3$ ) solution particle size 1  $\mu\text{m}$  was used, while the process is carried out using a rotatory source. All substrates were submitted a soap industrial cleaning next to the ultrasonic process with alcohol and acetone, it drying with compressed air.

### 2.2. Equipment, deposition and coatings characterization process

The multilayer coatings deposition process is carried out using a chamber r.f vacuum sputtering magnetron system designed and adapted by the University of Guadalajara Researchers. This system is equipped with four magnetrons and a rotary holder. The generation of plasma was made through to use of power supply d.c. Advanced energy brand. To carrier deposition of coatings A and B were obtained applying a current of 0.45 amperes, 456 V, and 461 V on target respectively. The previous deposition coatings are carried a high vacuum to  $3 \times 10^{-6}$  Torr. The work pressure was 11 and 69 mTorr, into chamber with a rate argon (Ar) and nitrogen ( $N_2$ ) gas of 60% and 40%, respectively. The substrates were put on rotatory holder sample are pre-heating around a temperature 200°C; these conditions deposition were reported previously by [9].

For optical properties is carried using by spectrometer Perkin Elmer using 4000 to  $400 \text{ cm}^{-1}$  range, it is plotting 2500 at  $400 \text{ cm}^{-1}$  with scanning number in a sample of 500, mirror speed at 100%. To obtain the Raman spectrum the Horiba Jobin Yvon model Libran HR distance focal of 800 mm, detector CCD analysis range  $300\text{-}2000 \text{ cm}^{-1}$  Raman shift, spectral resolution of 633 nm were used. Nanoindentation test, it is using a NANOVEA tribometer®, it is coupling a stylus indentator Bercovich diamond, it is applying a constant load of 20 mN. Oliver and Pharr's method was used to calculate the hardness. Tribology test, was obtained using a CSEM tribometer Instrument, applying a constant load of 10 N, using a ball steel chromium (100 Cr6) radius diameter 10 mm, displacement distance of 500 m, and linear speed of 0.52 m/s. The environmental conditions were a temperature of 18°C and 57 % humidity. Scratch test is carried out by the Multiscratch NANOVEA® equipment, applying progressive loads starting at 0.1 until 35 N, with relation load 14 N/ min, speed 1.404 mm/min using Rockwell nanoindentation stylus, coupling in focus camera to obtain images.

## 3. Discussion and results

### 3.1. Optical analysis

#### 3.1.1. FTIR spectra

In Fig. 1, for both coatings, it presents a bridging system of the  $W_2O$  the weak, and sometimes broad bands observed in

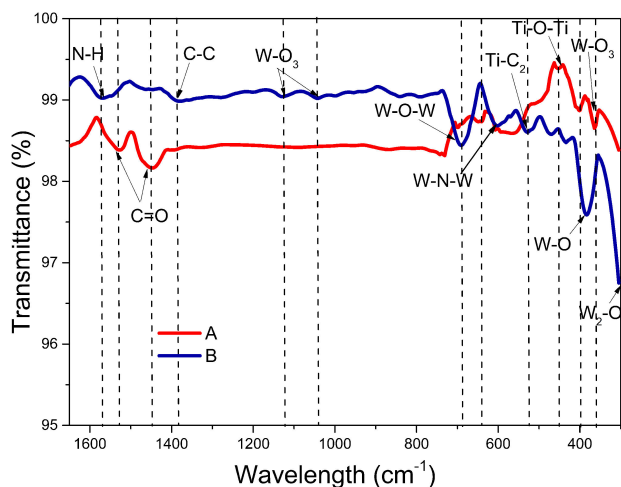


FIGURE 1. FTIR spectra of multilayer coatings A and B on corning glass deposited by DC magnetron sputtering.

the 400 to 300  $\text{cm}^{-1}$  range are then likely to be due to deformations of the tungsten-oxygen double bond systems, [9]. Also, three regions appear for the  $\text{WO}_3$  vibrations at 900-600  $\text{cm}^{-1}$ , 400-200  $\text{cm}^{-1}$ , and below 200  $\text{cm}^{-1}$ , [10]. In the frequency of 417  $\text{cm}^{-1}$ , it localized a weak band absorption corresponding to the bonding of W-O ( $\delta$  W-O), this peak is assigned stretching band [11,12]. In the frequency 560 to 460  $\text{cm}^{-1}$ , it presents the band absorption bending vibrations of Ti-O-Ti groups, [13]. In the frequency 555  $\text{cm}^{-1}$ , an absorption band is localized due to a stretching bond of  $\text{TiC}_2$  molecule in fundamental state at bond Ti-C<sub>2</sub>, [14]. Besides, it observes a weak band of asymmetric absorption the bond W-N-W, both coatings, [15]. In the bands situated at 679  $\text{cm}^{-1}$  and 805  $\text{cm}^{-1}$ , which are assigned to stretching vibrations  $\nu$  (W-O-W) of the bridging oxygen atoms, [16]. The frequency  $\sim 1030 \text{ cm}^{-1}$  is attributed at the presence of tungsten oxide ( $\text{WO}_3$ ), probably a consensus contamination by residual oxygen in chamber previous an ionic sputtering, [17]. In the absorption band located at  $\sim 1297 \text{ cm}^{-1}$  which is attributed to the C-C link stretching vibrations, [18]. Only the coating A to appear the low frequencies  $\sim 1459 \text{ cm}^{-1}$  of double bond oxygen-carbon (C=O) stretching vibration band, [19,20]. On the other hand, the band absorption assigned  $\sim 1650 \text{ cm}^{-1}$ , represents N-H bending vibrations, [21,23].

### 3.1.2. Raman spectra

Figure 2, shows the Raman spectrum in multilayer coatings W/WN, TiN/TiN, and W/TiN obtained by DC magnetron sputtering. As well known, the inorganic compound has vibrational bands mainly below 1500  $\text{cm}^{-1}$ . In Fig. 2 of coating A, presents a weak peak in the dispersion band assigned at 260  $\text{cm}^{-1}$  in the interval 250-435  $\text{cm}^{-1}$ , corresponding to transverse phonons (TA), of metallic ions vibrations of Ti for both coatings (A and B), [24]. In the frequency 520  $\text{cm}^{-1}$ , an intense peak (very sharp) of dispersion acoustic phonons appears; this is a characteristic crystalline silicon wafer, where

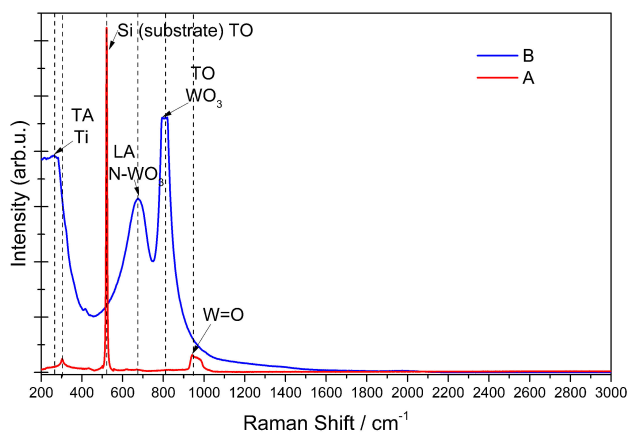


FIGURE 2. Raman spectra multilayer of coatings A and B on corning glass deposited by DC magnetron sputtering.

the angles, the power, and bonding energy are very ordered uniforms, [25], silicon like a diamond. It has only one first order Raman active phonon located at the Brillouin-zone center, long wavelength transverse optical phono (TO). On the other hand, at the 938  $\text{cm}^{-1}$ , a weak peak is observed, it indicates that Raman positions depended on the tungsten content, the higher frequency at which the band appears, and the removals of water cause a shift of Raman bands to higher frequency [12]. For the case of coating B, it localized a band of 658  $\text{cm}^{-1}$ , it is attributed to the N-Phase, while, it is interacting with the oxide tungsten ( $\text{WO}_3$ ), [276]. The frequency at 811  $\text{cm}^{-1}$  is assigned to the Raman band, characteristic of monoclinic  $\text{WO}_3$ . It was obtained and not changed as a function of temperature indicating the formation of highly stable monocrystalline  $\text{WO}_3$ , [27,28].

### 3.2. Nanoindentation test

In [29], he found the direct proportional relationship between hardness and modulus of elasticity, *i.e.*, greater hardness increases the elasticity of the material. To determine the hardness ( $H$ ), and the modulus of elasticity ( $E_r$ ), the Oliver and Fharr method is used, [30], it is described in the next Eq. (1).

$$H = \frac{P_{\max}}{A}, \quad (1)$$

where  $H$  is the coating's hardness  $P_{\max}$  is the maximum peak of indentation, and  $A$  is the area of the coating's footprint.

To calculate the resistance at plastic deformation (GPa), the next relation is used Eq. (2):

$$\frac{H^3}{Er^2}, \quad (2)$$

where  $H$  is the coating's hardness (GPa), and  $E_r$ , is the modulus of elasticity value of the material.

On the other hand, to calculate the elastic recovery (%), the next equation is used Eq. (3) [31]:

$$R = \frac{\delta_{\max} - \delta_P}{\delta_{\max}}, \quad (3)$$

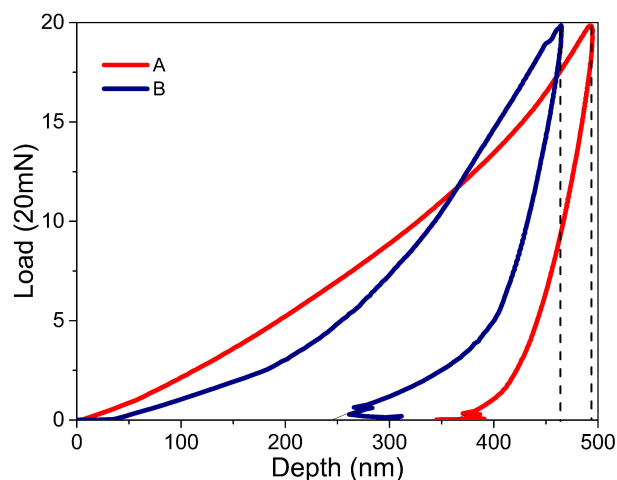


FIGURE 3. Typical nano-indentation curves (load) versus depth (nm) of multilayer coatings A and B on AISI 1060 deposited by DC magnetron sputtering.

where  $R$  is the elastic recovery (%),  $\delta_{\max}$  is the maximum displacement, and  $\delta_P$  is the plastic displacement.

Figure 3 shows the load and discharge curves of the nanoindentation tests for the multilayer A and B coating deposited by DC Sputtering. It can be seen that the A coating, applying a load of 20 mN, tends to penetrate to a depth of 500 nm. The material presents plastic deformation since the discharge curve does not return in the same direction in the load curve with a significant gradient between the two curves. However, for the case of coating B, the penetration is less than A (450 nm) and likewise, its plastic deformation is less. Table I shows the mechanical properties, while the results of the elasticity module and hardness are similar between them. However, coating B presents the best conditions of elasticity recovery (46 %) and maximum deformation resistance (5 %). The behavior of low hardness and the elastic module can be attributed by the surface fracture on coatings, it promoted compressible stress, due to the electron thermal diffusion, energy transfers to the lattice and heat is transported into WTi/Si target. Equalization of temperatures happened at approximately ten picoseconds. The thermalization properties of WTi thin film and Si substrate are quite different; thus, fast heating and cooling are presented, [32]. On the other hand, [33], mention in their research, that, the low hardness in multilayer coating is due to the amortization associated with important increase of W-O (W25O75) bonding ionic obtained hardness values of 7.7 GPa.

TABLE I. Mechanical properties of multilayer coatings A and B on AISI 1060 deposited by DC magnetron sputtering.

| Property                   | Coating       |               |
|----------------------------|---------------|---------------|
|                            | A             | B             |
| Hardness (GPa)             | $6.1 \pm 0.4$ | $5.5 \pm 0.4$ |
| Young's modulus (GPa)      | $171 \pm 16$  | $164 \pm 12$  |
| Elastic recovery (%)       | 28            | 46            |
| Deformation resistance (%) | 3             | 5             |

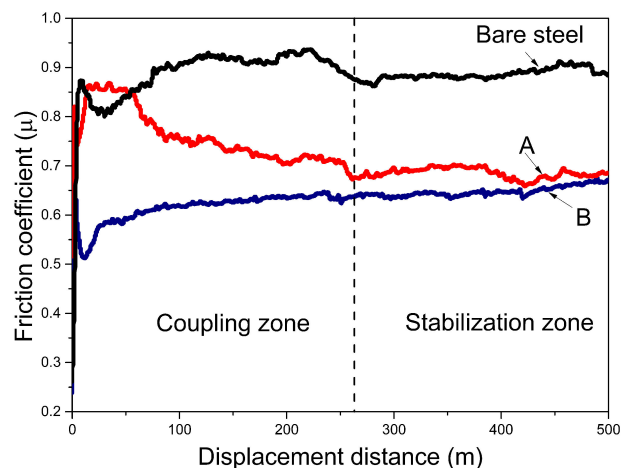


FIGURE 4. Friction coefficient curves versus displacement distance in coatings A and B on AISI 1060 deposited by DC magnetron sputtering.

### 3.3. Tribology test

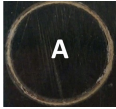

#### 3.3.1. Pin on disk test

Figure 4 shows the values friction coefficient (COF) and the wear loss in multilayer coatings on a steel carbon substrate. For the case of the bare substrate, it presents a COF of  $0.83 \pm 0.03$ , whose result is similar to the reported by [34]. Coating A, presents a little friction between coatings and the ball, allowing a COF below of  $0.70 \pm 0.04$ . Coating B presents a low COF of  $0.61 \pm 0.03$  compared with the bare substrate. These COF values are similar to those obtained by Polcar and collaborator's work [35], using an  $\text{Al}_2\text{O}_3$  ball as a counterpart reporting COF values in WN coatings of 0.6 and  $\text{W}_{87}\text{O}_{13}$  of 0.73. Another factor, the COF of uncoated substrate influences the composition in the microstructure of material in the steel. This due to the presence of austenite grains, with uniform carbide precipitation in the microstructure formed by the perlite phase and a ferrite phase and Eutectoid composition, [36-38]. The reason for the friction behavior using counterpart WN-100  $\text{Cr}_6$  is attributed to a combination of factors, such as the initial contact area, the chemical reactivity of the contact surface, and the formation of debris, [39]. Another factor, that has been reported, is the higher correlation directly COF versus roughness, thus, if the roughness increases, so do the COF, as well as, the generation of cracks on the top surface, promoting anti-slip agents to induce the increase of slide load and friction, [40,41]. In this case, morphological analysis of previous reported, the coating A and B have shown cracks with spheres domes sharp on the top surface; thus, it inducing increase COF [8].

#### 3.3.2. Calculation of wear rate

To calculate wear rate is uses the next equation considering WN density  $17.8 \text{ gr/cm}^3$ , the sliding distance of 500 m, an applicate load of 20 mN, [42,43].

TABLE II. Tribological properties of multilayer coatings A and B on AISI 1060 deposited by DC magnetron sputtering.

| Property   | Coating              |   |                      |   |
|--|----------------------|---|----------------------|---|
|  | A                    |   | B                    |   |
| Mass loss ( $w$ ) expressed in grams                   | 0.00137              |  | 0.00140              |  |
| Wear rate ( $W$ ) expressed in $\text{mm}^3/\text{Nm}$ | $7.7 \times 10^{-3}$ |   | $7.8 \times 10^{-3}$ |   |

$$W = \frac{\Delta w}{L\rho F}, \tag{4}$$

where  $W$  is wear rate in  $\text{mm}^3/\text{Nm}$ ,  $\Delta w$  loss weight in grams,  $L$  is the sliding distance in meters,  $\rho$  is coating density, and  $F$  is the load applicate.

In Table II, shows the mass loss and wear rate for coating A and B. For the case of coating A mass loss and wear rate were 0.00137 gr, and  $7.7 \times 10^{-3} \text{ mm}^3/\text{Nm}$  respectively. These results are similar to the ones obtained for the case of coating B, while values are 0.00140 gr., and  $7.8 \times 10^{-3} \text{ mm}^3/\text{Nm}$ , respectively. The values of mass loss and wear rate are high significantly can be influenced by the nature of the counterpart (100 Cr<sub>6</sub>) which tends to produce oxidation products with high and unstable friction. The variation in the instability of the friction process is due by wear particles (debris) expelled from the contact surface (as observed in the imagens of coating A and B).

3.3.3. Analysis contact pressure

To calculate medium contact pressure ( $P_o$ ), it uses the Hertz's in the next equation, [44] is used Eq. (5):

$$P_o = \frac{4}{3} \frac{E_{eff}}{\pi} \frac{a}{R}, \tag{5}$$

Where  $P_o$  corresponding contact pressure, and rate ( $a/E_{eff}$ ) indicating the deformation of material produced during the test. If contact pressure is less than Young's modulus itself material, then is produced a deformation elastic on coating; on the contrary case is carried a plastic deformation.

In Table III shows the values of Hertz's contact stress. The maximum Hertzian contact pressure for coating A is 0.924 GPa, value similar for the coating B, which result is 0.910 GPa. This values compared their Young's modulus is less, thus, does exist deformation elastic in the system pare tribomechanical.

TABLE III. Values of contact pressure using Hertz's equation.

| Materials type                    | Young's modulus (GPa) | Poisson coefficient ( $\nu$ ) | Maximum Hertzian contact pressure (GPa) |
|-----------------------------------|-----------------------|-------------------------------|---|
| Steel ball (100 Cr <sub>6</sub> ) | 200                   | 0.30 [45]                     | -                                       |
| Coating A                         | $171 \pm 16$          | 0.29 [35]                     | 0.924 [46]                              |
| Coating B                         | $164 \pm 12$          | 0.29                          | 0.910                                   |

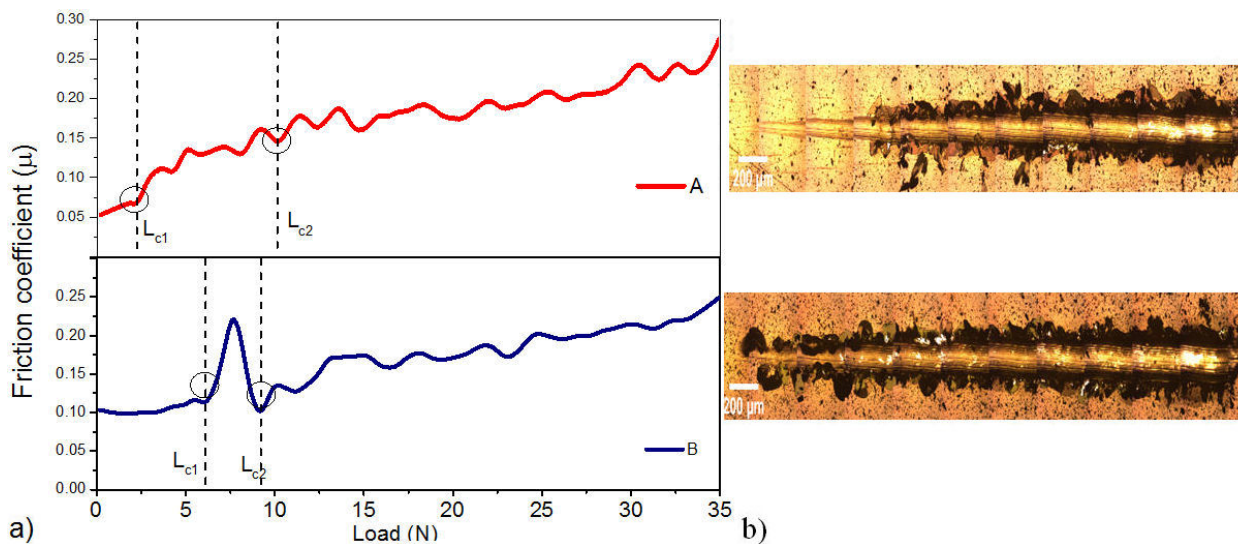


FIGURE 5. a) Friction coefficient curves versus load (N); b) wear on the track analysis in multilayer coatings A and B on AISI 1060 deposited by DC magnetron sputtering.

### 3.4. Scratch test

Figure 5(a-b) shows the behavior of the multilayer scratch test of coatings A and B on AISI 1060 deposited by DC magnetron sputtering. Figure 5a, shows the friction coefficient curves in function at the increase of load. It is observed in coating A that the critical load ( $L_{C1}$ ) is causing damage around 2 N and the second load localized ( $L_{C2}$ ) coating detachment at 7 N. For the case of coating B, a sliding friction curve a peak is observed when a 7 N load is applied. This peak is attributed by the presence of spherical cones containing diverse hardness properties. For Fig. 5b, in all the cases, the evolution of the power Hertziana (dark shadow) is observed and produced for the application of progressive loads. Three main fails modes in the coating are identified; a) Irregular edges with longitudinal shading trajectory across the track ( $L_{C1}$ ) at 0 - 2.3 N load, which is associated with the onset of Chevron-type cracking [47], indicating a cohesion failure in the coating; b) Semi-circular edge material peeling off the track with a diameter of  $\sim 100 \mu\text{m}$  ( $L_{C2}$ ) when a load of 7.4 N is applied associated with the onset of chipping failure extending from tensile arc cracks, indicating adhesive failure between the coating and the substrate; and finally c) Coating detachment within the test track with loads greater than 10.7 N is observed- 35 N [48-50].

## 4. Conclusions

FTIR spectra analysis has shown absorption bands of W-O (tungsten oxide) and oxygen-carbon double (C=O) interactions typical in the deposition by PVD. Raman spectra analy-

sis confirmed the presence of a weak peak of Ti metallic ion vibrations a low frequency and dispersion band corresponding to bonding  $\text{WO}_3$  monoclinic. The hardness properties by nanoindentation, shown low improvement; however, it is better than bare steel (AISI 1060). The tribology test by a pin on a disc, shown similar values of COF in 0.65 to 0.85 for both coatings. This behavior can due probably the unsuitable selection of ball (steel 100 Cr<sub>6</sub>), promoting the generation debris by contact. Another factor is the due presence of cracks and spherical domes on the surface top in both coatings. The mass loss and wear rates showed high values in the two coatings. For Scratch test were identified three mechanics of wear: a) Irregulars border appear dark shadow (chevron); b) Semicircle detachment on track and c) Centre detachment on way track in function to displacement. For improvement tribo mechanical properties, it recommended decreases thickness to three micres to eliminate tension stress.

## Acknowledgments

The author is grateful for the CONACYT post-grade fellowship. Thanks are also given to Ph.D. García Alamilla Ricardo, from the Center of Petrochemical Investigation, TecNM/Instituto Tecnológico de Ciudad Madero, Parque Tecnia (Pequeña y Mediana Industria) Bahía Aldair Altamira Mexico, for supporting the FTIR analysis. Gratitude towards Ph.D. Sion Federico Olive Méndez of Advanced Materials Research Center S. C., CIMAV, Miguel de Cervantes 120, Chihuahua Industrial Complex, C.P. 31136, Chihuahua, México, for providing Raman spectrum analysis.

1. M.J. Neale, M. Gee, *A Guide to Wear Problems and Testing for Industry*. William Andrew. Applied Science Publisher (2001) 3-31. <https://doi.org/10.1016/B978-081551471-8.50002-5>
2. J. Morales-Hernández, A. Mandujano-Ruíz, Torres-González, F.J. Espinoza-Beltrán, H. Herrera-Hernández, Low friction coefficient coatings Ni-Cr by magnetron sputtering, DC. *Rev. Metal.* **3** (2015) 1-8. <http://dx.doi.org/10.3989/revmetalm.047>
3. J. E. Sundgren, Formation and characterization of titanium nitride and titanium carbide films prepared by reactive Sputtering. *Dissertation Linköping* **79** (1982) 13. [https://inis.iaea.org/collection/NCLCollectionStore/\\_Public/13/693/13693374.pdf](https://inis.iaea.org/collection/NCLCollectionStore/_Public/13/693/13693374.pdf)
4. M. Wen, Q.N. Meng, W.X. Yu, W.T. Zheng, S.X. Mao, M.J. Hua, Growth, stress and hardness of reactively sputtered tungsten nitride thin films. *Surface and Coatings Technology* **205** (2010) 1953-1961. <https://doi.org/10.1016/j.surfcoat.2010.08.082>
5. R.F. Londoño Menjura *et al.*, Influence of deposition temperature on WTiN coatings tribological performance. *Applied Surface Science* **427** (2018) 1096-1104. <https://doi.org/10.1016/j.apsusc.2017.07.215>
6. M. Albella Jose. Láminas delgadas y recubrimientos: Preparación, propiedades y aplicaciones. *Consejo Superior de Investigaciones Científicas*. Madrid España (2003) 559-560.
7. D.I. James, *Surface damage caused by Polyvinyl Chloride Sliding on Steel*. *Wear* **2** (1958) 183-194. [https://doi.org/10.1016/0043-1648\(59\)90003-1](https://doi.org/10.1016/0043-1648(59)90003-1)
8. A. González, M. Flores, J.C. Caicedo, W. Aperador and A.B. Morales-Cepeda, Síntesis y caracterización electroquímica de recubrimientos de multicapas metal cerámico de W/WN, Ti/TiN y WTiN. *Rev. Mex. Fis.* **64** (2018) 368-374. <https://doi.org/10.31349/RevMexFis.64.368>
9. W. Douglas Timothy, *Infrared and Raman spectra of metal-oxygen complexes*. Thesis doctor of philosophy of University of London, chemistry department Imperial College, south Kensington (1967) 58. <https://spiral.imperial.ac.uk/bitstream/10044/1/17628/2/Wickens-TD-1967-PhD-Thesis.pdf>
10. M.F. Daniel, B. Desbat, J.C. Lassegues, B. Gerand, M. Figlarz. Infrared and Raman study of  $\text{WO}_3$  tungsten triox-

- ides and WO<sub>3</sub>, xH<sub>2</sub>O tungsten trioxide hydrates. *J. Solid State Chemis.* **67** (1987) 235-247. [https://doi.org/10.1016/0022-4596\(87\)90359-8](https://doi.org/10.1016/0022-4596(87)90359-8)
11. I. Hargittai, M. Hargittai, V.P. Spiridonov and E.V. Erokhin, *J. Mol. Structure* **8** (1971) 31-41. [https://doi.org/10.1016/0022-2860\(71\)80039-X](https://doi.org/10.1016/0022-2860(71)80039-X)
  12. J. Díaz-Reyes, V. Dorantes-García, A. Pérez-Benítez, J.A. Balderas-Lopez, Obtaining of films of tungsten trioxide (WO<sub>3</sub>) by resistive heating of a tungsten filament. *Superficies y Vacío sociedad Mexicana de Ciencia y Tecnología de superficies y materiales* **21** (2008). <http://www.scielo.org.mx/pdf/sv/v21n2/v21n2a3.pdf>
  13. T. Mahalingan, C. Selvakumar, E. Ranjith Kumar, T. Venkatachalam, Structural, optical, morphological and thermal properties of TiO<sub>2</sub>-Al and TiO<sub>2</sub>-Al<sub>2</sub>O<sub>3</sub> composite powders by ball melting. *Phys. Lett. A*, **381** (2017) 1815-1819. <https://doi.org/10.1016/j.physleta.2017.02.053>
  14. W. Xue-Bin, D. Chua-Fan and W. Lai-Sheng, Vibrationally Resolved Photoelectron Spectra of TiCx- (x =2-5) Clusters. *J. Phys. Chem. A* **101** (1997) 7699-7701. <https://doi.org/10.1021/jp971838k>
  15. L. Addonizio Maria, C. Anna, A. Alessandro, G. Emilia and L. Laura, Influence of process parameters on properties of reactively sputtered tungsten nitride thin films. *J. Vac. Sc. Technol. A*, **30** (2012) 031506-1-031506-8. <https://doi.org/10.1116/1.3698399>
  16. B. Pecquenard, h. Lecacheux, j. Livage, and c. Julien, Orthorhombic WO<sub>3</sub> formed via a ti-stabilized WO<sub>3</sub> 1/3h<sub>2</sub>o phase. *J. Solid State Chemis.* **135** (1998) 159-168. <https://doi.org/10.1006/jssc.1997.7618>
  17. P. Hoffman, H. Galindo, G. Zambrano, C. Rincón, FTIR studies of tungsten carbide in bulk material and thin film samples. *Material Characterization* **50** (2003) 255-259. [https://doi.org/10.1016/S1044-5803\(03\)00100-1](https://doi.org/10.1016/S1044-5803(03)00100-1)
  18. M. Morsi Abou Sekkina and S. Samy Asar, Infrared absorption Spectra and hydrogen bonding of some solid aninoanthraquinones. *Proc. Indian Nath. Sci. Acad.* **48** (1982) 112-118. <https://insa.nic.in/UI/Journalarticle.aspx?jid=NA=&&VID=Mjky&IsNm= SXNzdWUgMUEGICAg>
  19. G. Davindson, Spectroscopic properties of inorganic and organometallic compounds. *The Royal Society of Chemistry*. First edition, **30** (1997) 349. <https://doi.org/10.1080/00945717708069725>
  20. H. Barbara Stuart, J. David Ando, *Biological Applications of Infrared Spectroscopy*. (John Wiley and Sons editorial, first edition 1997) 61. ISBN: 978-0-471-97414-7
  21. W.L. Scopel, M.C. Fantini, M.I. Alayo, I. Pereyra, *Thin solid films* **413** (2002) 59-64. [https://doi.org/10.1016/S0040-6090\(02\)00346-2](https://doi.org/10.1016/S0040-6090(02)00346-2)
  22. F. Giorgis, C.F. Pirri, E. Tresso, *Thin solid films* **307** (1997) 298-305. [https://doi.org/10.1016/S0040-6090\(97\)00272-1](https://doi.org/10.1016/S0040-6090(97)00272-1)
  23. M.M. Ismael, The effect of silicon orientation on Thickness and chemical bonding configuration of SiO<sub>x</sub>N<sub>y</sub> thin films. *International Letters of Chemistry, Physics and Astronomy*, **19** (2013) 1-9. <https://www.infona.pl/resource/bwmeta1.element.baztech-7f6c119c-7831-4304-9816-b5769f4d4de9/tab/summary>
  24. B.O. Francisco, J. B.G. Gilberto, G.B.A. Maryory, Influence of the duplex coatings on the mechanical properties and wear resistance of the tempered AISI 4140 steel. *Journal EIA Volume* **19** (2013) 151-160. <http://www.scielo.org.co/scielo.php?script=sci.arttext&pid=S1794-12372013000100014>
  25. P.G. Spizzirri, J.H. Fang, E. Gauja and S. Prawer, Nano-Raman spectroscopy of silicon surfaces. Research Gate Article in materials Forum (2010). <https://arxiv.org/ftp/arxiv/papers/1002/1002.2692.pdf>
  26. M. Filipescu, V. Ion, D. Colceag, P. M. Ossi, M. Diniescu, Growth and characterizations of nanostructured tungsten oxides. *Romanian Reports in Physics Supplement* **64** (2012) 1213-1225. <https://core.ac.uk/download/pdf/74312823.pdf>
  27. W. Bhalchandra Anil, *Synthesis of porous monoclinic tungsten oxides and their applications in sensor*. Thesis Doctoral Philosophy in chemistry, University of Maine (2003). <https://pdfs.semanticscholar.org/bd3e/3fad72a065e04d13e5934ab20bd7bb639dd7.pdf>
  28. K. Srinivasarao and P.K. Mukhopadha, IR and Raman Studies on r.f. magnetron sputtered nano crystalline WO<sub>3</sub> thin films. *Int. J. App. Eng. Res.* **16** (2015) 36148-36156. ISSN 0973-4562 [https://www.researchgate.net/publication/283108627\\_IR\\_and\\_Raman\\_studies\\_on\\_rf\\_magnetron\\_sputtered\\_nano\\_crystalline\\_WO3\\_thin\\_films](https://www.researchgate.net/publication/283108627_IR_and_Raman_studies_on_rf_magnetron_sputtered_nano_crystalline_WO3_thin_films)
  29. G.S. Kim, S.Y. Lee and J.H. Hahn, *Surf. Coat. Technol.* **171** (2003) 91. [https://doi.org/10.1016/S0257-8972\(03\)00244-5](https://doi.org/10.1016/S0257-8972(03)00244-5)
  30. W.C. Oliver and G. Pharr, An improved Technique for determining hardness and elastic modulus using load displacement sensing indentation experiments. *J. Mater Res.* **7** (1992) 1564. <https://doi.org/10.1557/JMR.1992.1564>
  31. V. Hajek, K. Rusnak, J. Viecek, L. Martinu and H.M. Hawthorne, *Wear* **213** (1997) 80. [https://doi.org/10.1016/S0043-1648\(97\)00176-2](https://doi.org/10.1016/S0043-1648(97)00176-2)
  32. S. Petrović *et al.*, Picosecond Laser Ablation of Nano-Sized WTi thin film. *Laser Physics* **19** (2009) 1844-1849. <https://doi.org/10.1134/S1054660X09150>
  33. T. Polcar, A. Cavaleiro, Structure, mechanical properties and tribology of W-N and W-O coatings. *Int. Journal of Refractory Metals and Hard Materials* **28** (2010) 15-22. <https://doi.org/10.1016/j.ijrmhm.2009.07.013>
  34. C.C. Viátara, M.I. Castro, J.M. Vélez, A. Toro, Unlubricated sliding wear of pearlitic and bainitic steels. *Wear* **259** (2005) 405-411. <https://doi.org/10.1016/j.wear.2005.02.013>
  35. T. Polcar, N.M.G. Parreira, A. Cavaleiro, Structural and tribological characterization of tungsten nitride coatings at elevated temperature. *Wear* **265** (2008) 319-326. <https://doi.org/10.1016/j.wear.2007.10.011>

36. A. García, á. Varela, J.L. Miel, C. Camba, F. Barbadillo, *Estudio tribológico de aceros austeníticos tipo Hadfield: influencia del manganeso en su respuesta frente al desgaste. Revista de metalurgia*, **46** (2010) 47- 52. <http://revistademetalurgia.revistas.csic.es/index.php/revistademetalurgia/article/view/1158>
37. K. Sipos, M. López, and, M. Trucco. Surface martensite White layer produced by adhesive sliding wear-friction in AISI 1065 steel. *Rev. Lat. Mat.* **28** (2008) 46-50. [http://ve.scielo.org/scielo.php?script=sci\\_arttext&pid=S0255-69522008000100006](http://ve.scielo.org/scielo.php?script=sci_arttext&pid=S0255-69522008000100006)
38. G. Frade Rubén. *Prácticas de elementos amovibles y fijos no estructurales* (2014). <https://fradeblogs.wordpress.com/2014/02/01/los-aceros/>
39. M.F. Cano Ordoñez, J.S. Restrepo Paruma, F. Sequeda Osorio, *The effect of counterpart material on the sliding wear of TiAlN coatings deposited by reactive cathodic pulverization. SCI. CUM IND.* **3** (2015) 59-66. <http://dx.doi.org/10.18226/23185279.v3iss2p59>
40. N.L. Parthasarathi, U. Borah, S.H. K. Albert, Correlation between coefficient of friction and surface roughness in dry sliding wear of AISI 316 (N) Stainless Steel elevated Temperatures. *Computer Modelling and new Technologies* **17** (2013) 51-63. <https://www.semanticscholar.org/paper/CORRELATION-BETWEEN-COEFFICIENT-OF-FRICTI-ON-AND-IN-Parthasarathi-Borah/d5bd514436b05fb9b8af5ab57476cba71a7470d6>
41. B. Ivković, M. Djukđjanović, D. Stamenković, The influence of the contact surface roughness on the static friction coefficient. *Tribology in industry*, **22** (2000) 41- 44. <http://www.tribology.rs/journals/2000/2000-3-4.html>
42. S.R. Chauhan, K. Dass, Dry sliding wear behaviour of Titanium (grade 5) alloy by using response surface methodology. *Advances in Tribology e* **2** (2013) 1-9. <https://doi.org/10.1155/2013/272106>
43. ASTM G99-05. Standard Test Method for Wear Testing with a Pin-on-Disk Apparatus. Copyright ©ASTM International, 100 Barr Harbor Drive, PO Box C700, West Conshohocken, PA 19428-2959. United States (2010). <https://www.astm.org/DATABASE.CART/HISTORICAL/G99-05.htm>
44. C. Fischer-Cripps Antony, *Introduction to contact mechanics*. In chapter 6: Elastic contact, 6.1 Hertz contact equations Second edition, Springer Science, printed in United Sates of America (2007) 101-108. ISBN 978-0-387-68187-0
45. A.G. Mamalis, A.S. Branis, D.E. Manolakos. Modelling of precision hard cutting using implicit finite element methods. *Journal of Materials Processing Technology* **123** (2002) 464-475. [https://doi.org/10.1016/S0924-0136\(02\)00133-4](https://doi.org/10.1016/S0924-0136(02)00133-4)
46. Hertzian contact stress calculator. *Hertzian contact stress calculator online*. <https://amesweb.info/HertzianContact/HertzianContact.aspx> (consulted 4 April 2020).
47. ASTM C1624, Método de prueba estándar para resistencia a la adhesión y los modos de fallo mecánico de los recubrimientos cerámicos por cuantitativa de punto único del rasguño de pruebas ASTM International, West Conshohocken, PA, (2015). <https://www.astm.org/Standards/C1624.htm>
48. ASTM 171, *Standard Test Method for Scratch Hardness of Materials Using a Diamond Stylus*. West Conshohocken, PA United States (2003). <https://www.astm.org/DATABASE.CART/HISTORICAL/G171-03.htm>
49. A. Mubarak, E. Hamzah, Influence of nitrogen gas flow rate on the microstructural and mechanical properties of TiN deposited carbon steel synthesized by CAE PVD Technique. *AJSTD* **23** (2006) 239-251. <https://doi.org/10.29037/ajstd.111>
50. J.C. Caicedo, W. Aperador and Y. Aguilar, Tribological performance evidence on ternary and quaternary nitride coatings applied for industrial steel. *Rev. Mex. Fis.* **59** (2013) 364-370 [http://www.scielo.org.mx/scielo.php?pid=S0035-001X2013000400012&script=sci\\_arttext&tlng=pt](http://www.scielo.org.mx/scielo.php?pid=S0035-001X2013000400012&script=sci_arttext&tlng=pt)